ACS APPLIED MATERIALS & INTERFACES

Research Article

www.acsami.org

Alternative Spectral Photoresponse in a *p*-Cu_2ZnSnS_4/*n*-GaN Heterojunction Photodiode by Modulating Applied Voltage

Gang Yang,[†] Yong-Feng Li,*[,†,‡] Bin Yao,*[,†,‡] Zhan-Hui Ding,[†] Rui Deng,[§] Xuan Fang,[∥] and Zhi-Peng Wei[∥]

[†]State Key Lab of Superhard Materials and College of Physics, Jilin University, Changchun 130012, People's Republic of China

[‡]Key Laboratory of Physics and Technology for Advanced Batteries (Ministry of Education), College of Physics, Jilin University, Changchun 130012, China

[§]School of Materials Science and Engineering, Changchun University of Science and Technology, Changchun 130022, China

[∥]State Key Laboratory on High-Power Semiconductor Lasers, Changchun University of Science and Technology, 7186 Wei-Xing Road, Changchun 130022, China

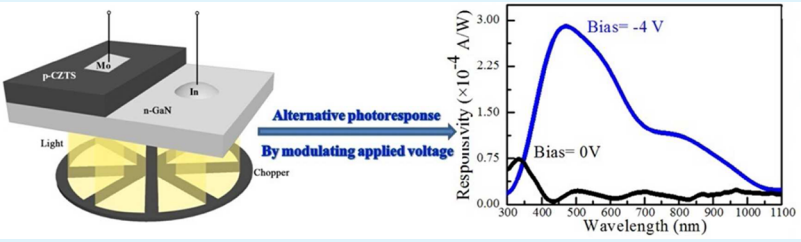

ABSTRACT: We report alternative visible and ultraviolet light response spectra in a p-Cu_2ZnSnS_4 (p-CZTS)/n-GaN heterojunction photodiode. A CZTS film was deposited on an n-GaN/sapphire substrate using a magnetron sputtering method. Current−voltage characteristic of the p-CZTS/n-GaN heterojunction photodiode showed a good rectifying behavior. The spectral response measurements indicate that the response wavelength of the photodiode can be tuned from ultraviolet to visible regions via applying zero and reverse bias. A band alignment at the interface of the p-CZTS/n-GaN heterojunction was proposed to interpret the spectral response of the device.

KEYWORDS: *photodiode, GaN, magnetron sputtering, Cu_2ZnSnS_4, heterojunction*

INTRODUCTION

Solar energy is considered to be the most economic and effective available renewable energy resources.[1−3] Photovoltaic (PV) cells including thin film solar cells,[4] dye-sensitized solar cells,[5] organic bulk junction solar cells,[6] and hybrid perovskite solar cells[7,8] have been widely investigated because they can convert sunlight directly into electricity. In recent years, the kesterite Cu_2ZnSnS_4 (CZTS) emerged as a potential p-type material used in thin film photovoltaic applications.[9−12] It has an ideal direct bandgap of about 1.5 eV and a large absorption coefficient (>10^4 cm^{-1}).[13,14] The use of only nontoxic and abundant elements makes it to be more environmental friendly and economical compared with CdTe and $Cu(In_{1-x}Ga_x)Se_2$.[15,16] Recently, various deposition techniques including vacuum and nonvacuum methods were applied to fabricate CZTS solar cells, and the power conversion efficiency (PCE) record has been updated rapidly.[17−19]

A typical structure of CZTS solar cells is Mo/CZTS/CdS/ZnO/ZnO:Al/Al.[11] The n-type CdS buffer layer is fabricated on the p-type CZTS absorption layer to form a p−n junction, where carriers are separated as light irradiates. The wide bandgap semiconductors including an intrinsic ZnO and a heavily n-doped ZnO:Al were usually used as the window layer, which reduces the series resistance of solar cells.[20] Recently, researches also focused on direct deposition of n-type wide-bandgap ZnO on p-type CZTS to form Cd-free p-CZTS/n-ZnO heterojunction devices.[21,22] Htay et al. reported the higher open circuit voltage (V_{oc}) and relative quantum efficiency at the short wavelength regions in the p-CZTS/n-ZnO heterojunction solar cells than those using CdS as the buffer layer.[23] They ascribed these to the higher built-in potential induced by the wider bandgap ZnO and the increase of transparency. In addition, the proposed type-I band alignment of CZTS/ZnO heterojunction (i.e., the conduction band of CZTS is lower than that of ZnO) can reduce the recombination rate greatly. Among lots of wide-bandgap semiconductors, gallium nitride (GaN) has the same wurtzite structure with ZnO and similar wide direct bandgap (3.4 eV).[24,25] But few reports were available for the CZTS/GaN heterojunction. Due to the advantages of high saturation velocity (2.7×10^7 cm/s), radiation hardness, tolerability of aggressive environments, and a more mature processing technique, GaN was widely used for fabricating photodetectors.[26−28] More importantly, the type-I band alignment of the CZTS/GaN interface with a small

Received: May 17, 2015
Accepted: July 16, 2015
Published: July 16, 2015

DOI: 10.1021/acsami.5b04287
ACS Appl. Mater. Interfaces 2015, 7, 16653−16658

conduction band offset benefits to carrier separation and transport at the interface, so a p-CZTS/n-GaN heterojunction photodetector is expected to be a promising device with high performance.

In this work, we adopted the radio frequency (rf) magnetron sputtering method to fabricate a p-CZTS/n-GaN heterojunction photodiode and different biases were applied on the heterojunction to research the photoresponse. Interestingly, the device can alter spectral photoresponse by modulating applied voltage. The band diagrams of the heterojunction and the carrier diffusion process were used to explain this phenomenon.

EXPERIMENTAL SECTION

A p-type CZTS layer was deposited on a commercial available n-type GaN/sapphire substrate using radio frequency (rf) magnetron sputtering method to form a p-CZTS/n-GaN heterojunction. The electron concentration and the mobility of GaN are 4.54×10^{18} cm^{-3} and 233 cm^2V^{-1} s^{-1}, respectively, which are comparable with the properties of GaN in high performance devices. Finely mixed Cu_2S, ZnS, and SnS_2 powders with a molar ratio of 1:1:1 were pressed under 28 MPa at 700 °C for 30 min to form a ceramic CZTS target. In the whole sputtering process, the substrate temperature was fixed at 500 °C and Ar was used as the working gas with a pressure of 0.1 Pa. The base pressure of the sputtering chamber was 7.5×10^{-4} Pa, and the substrate to target distance was 60 mm. The sputtering power and time were 60 W and 60 min, respectively. The sample was annealed to improve the crystallinity and the stability of the electrical properties, after the deposition of CZTS on the GaN. The sample was located in a graphite box with 60 mg S powders and then transported into a rapid thermal processing furnace with nitrogen gas flow at normal pressure. The furnace was heated to 560 °C with a heating rate of 5 °C/s and finally maintained at this temperature for 15 min. After sulfuration, the sample was cooling down to room temperature naturally. A schematic diagram of heterojunction photodetector based on p-CZTS/n-GaN is shown in Figure 1a. Molybdenum (Mo) was deposited on the CZTS layer by the magnetron sputtering method for ohmic contact because it is usually used as the back contact in the CZTS-based solar cells and shows good ohmic contact with CZTS. Indium (In) metal was used as the n-type contact to n-GaN layer; it was pasted on the surface of GaN film, and then heated on a hot plate, whose temperature was fixed at 280 °C and lasted for 3 min. The process was operated in a glovebox in order to avoid the oxidation of the sample. A Xe lamp with a power of 150 W was used as the light source. First, the light passes through a chopper, and then enters into a spectrograph for obtaining monochromatic light with wavelength from 300 to 1100 nm, and the photodiode is illuminated from the n-GaN side, as shown in Figure 1a. The ultraviolet (UV) light can be absorbed by the GaN layer, and the visible light will pass through the GaN layer and be absorbed in p-CZTS.

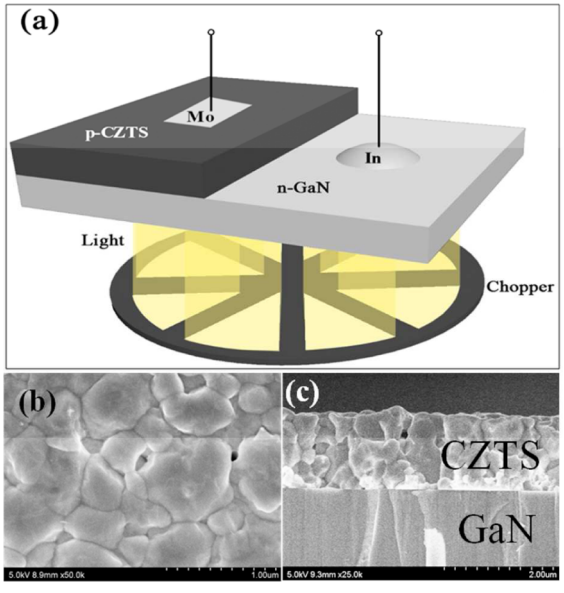

Figure 1. (a) Schematic illustration of the p-CZTS/n-GaN heterojunction photodiode. (b) Surface and (c) cross-sectional SEM images of the CZTS film fabricated on the GaN/sapphire substrate.

Crystalline structures of the films were characterized using Rigaku D/Max-RA X-ray diffractometer (XRD) with Cu Kα radiation (λ = 1.5406 Å). Surface morphology of the films was detected by field emission scanning electron microscopy (FESEM). Optical absorption spectra of the films were taken using an UV−visible spectrophotometer of UV-3101PC (Shimadzu, Kyoto, Japan). The current−voltage curves were measured at room temperature to further verify the formation of the p-n heterojunction. A standard lock-in amplifier technique was employed for the spectral response measurements.

RESULTS AND DISCUSSION

Figure 1b shows a typical SEM image of the CZTS film. It is found that the grain sizes are above 1 μm after annealing, and the surface is smooth; no pinholes or cracks were observed. Large grain sizes obtained by a rapid annealing processing can reduce the grain boundaries and the carrier recombination. Figure 1c shows a cross-sectional SEM picture of a typical CZTS/GaN heterojunction, the thickness of the CZTS layer is about 1.5 μm, and the CZTS layer is adhered well with the n-type GaN/sapphire substrate.

Figure 2 shows the XRD patterns of the CZTS thin film grown on the soda-lime glass (SLG) substrate, GaN substrate,

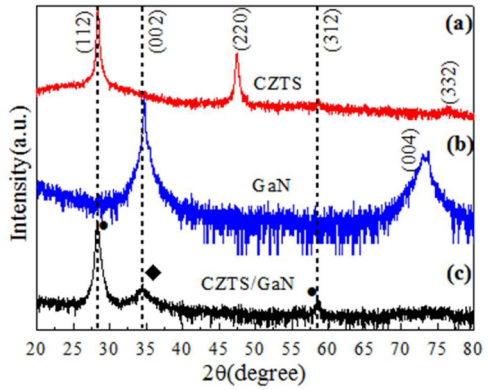

Figure 2. XRD patterns of (a) p-type CZTS grown on SLG substrate, (b) n-type GaN substrate, and (c) p-type CZTS thin films grown on the n-type GaN substrate.

and CZTS thin film directly grown on the GaN substrate. For the CZTS layer grown on the SLG substrate, three diffraction peaks located at 28.38°, 47.51°, and 58.56° are indexed as (112), (220), and (312), which belong to the kesterite structure of CZTS (JCPDS26-0575) with polycrystalline nature.[29] For the GaN substrate, only the (002) and (004) diffraction peaks are observed, indicating that the films have single wurtzite phase with obviously preferred orientation. For the CZTS thin films directly grown on GaN, no second phases were observed except the characteristic diffraction peaks for CZTS and GaN. Compared with the CZTS film grown on SLG substrate, the (220) diffraction peak at about 47.51° vanished, which is due to the different substrates used. It should be noted that no secondary phases are observed, implying that these thin films are single phase.

DOI: 10.1021/acsami.5b04287
ACS Appl. Mater. Interfaces 2015, 7, 16653−16658

The current−voltage (I−V) characteristics of the photodiode were measured at room temperature. As shown in Figure 3.

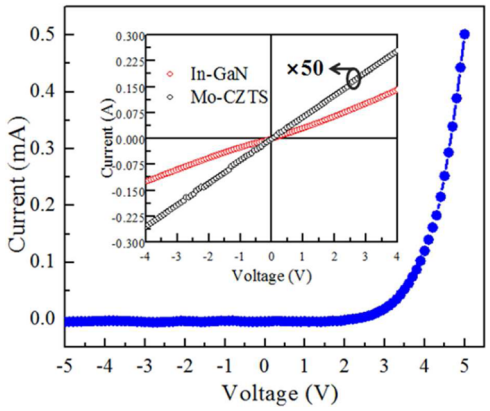

Figure 3. Current−voltage curve of the p-CZTS/n-GaN heterojunction. The inset shows the I−V characteristics of indium contacts on the n-GaN substrate and Mo contacts on p-CZTS.

The p-CZTS/n-GaN heterojunction shows an obvious rectifying behavior with rectification ratio ($I_{forward}/I_{reverse}$) of about 1.8×10^2 at 5 V in the dark, indicating the formation of a p−n junction diode. The turn-on voltage and the reverse leakage current are found to be 3.75 V and 1.95×10^{-6} A at −5 V, respectively. On the basis of a thermionic-emission (TE) model, the electrical characteristics of a diode can be calculated (for $qV > 3kT$) with the aid of the following equation:

$$I = I_0 \exp\left[\frac{q}{nkT}(V - IR_s)\right]$$

where I_0 is saturation current, V is applied voltage, R_s is series resistance, n is the ideality factor, T is experiment temperature in Kelvin, q is the electronic charge, and k is the Boltzmann constant. The series resistance (R_s) and the ideality factor (n) are very important parameters which impact the electrical characteristics of the diodes. These two values can be calculated using the equation $(dV)/[d(\ln I)] = [(nkT)/q] + IR_s$. In accordance with the data in the I−V characteristics, the obtained values were 1.5×10^4 Ω and 4.13, respectively. The large series resistance was attributed to the physics contact between the two layers, and the high density structural defects which serve as the recombination centers,[30] such as bulk defects in p-CZTS which are derived from the deviation of stoichiometric ratio and formed during growth of the film and surface defects derived from large lattice parameter mismatch between CZTS and GaN. In addition, large series resistance is responsible for the high turn-on voltage which is related to the large ideality factor. An optimization of the growth condition and some surface treatment should be used to improve the device performance in the future work. The inset of Figure 3 shows the I−V plots from the In-n-GaN and Mo-p-CZTS contact. The linear trend indicated that all the electrodes exhibited good ohmic contact, implying that the rectifying behavior originates from the p-CZTS/n-GaN junction instead of the Schottky contacts.

The room temperature optical absorption spectra of the CZTS grown on SLG substrate and GaN substrate are shown in Figure 4a. For the n-GaN substrate, a steep absorption edge at 365 nm is observed, which is in accordance with the previous reports.[31] The absorption spectrum of the CZTS film presents

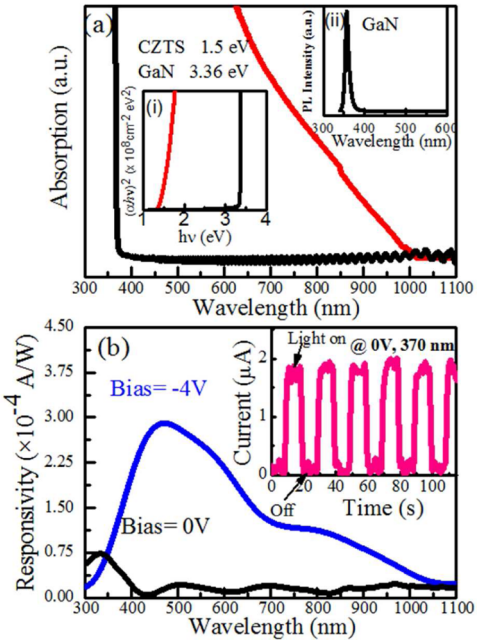

Figure 4. (a) Optical absorption spectra obtained at room temperature of the CZTS film (red) and GaN film (black). The insets show (i) the calculated bandgap of the CZTS and GaN films, and (ii) the room temperature PL spectra of n-GaN. (b) Spectral response of the p-CZTS/n-GaN photodiode at reverse biases of 0 and 4 V. The inset in (b) shows the time-dependent response of the device at zero bias.

an absorption edge at about 800 nm, which is consistent with the bandgap of CZTS. The bandgaps (E_g) of the CZTS and GaN films were determined to be 1.50 and 3.36 eV, respectively, as shown in the inset of (i) of Figure 4a. The room temperature photoluminescence (PL) spectra of the n-GaN is shown in the inset of (ii); only a dominant sharp near band edge emission peak at 356 nm is observed, which indicates the high quality of n-GaN.

To investigate the photoresponse properties of the p-CZTS/n-GaN heterojunction, spectral responses at zero and the reverse bias of 4 V were measured at room temperature. Figure 4b shows the photoresponse spectra of the heterojunction irradiated from the n-type GaN side when applying zero bias (black curve) and reverse bias (blue curve). When the applied bias is zero, a low responsivity is observed, and the peak responsivity is determined to be about 7.5×10^{-5}A/W at 340 nm, which is consistent with the absorption edge of the GaN substrate. The low responsivity is ascribed to the flow of the minority carriers (holes) dominating the photocurrent and the interface defects leading to carrier recombination. No photoresponse properties were observed at the forward bias, which is due to a narrower space charge region as applied forward bias. When the reverse bias of 4 V was applied on this device, the peak responsivity of the photodetector reaches about 3×10^{-4} A/W with a wide response range from 400 to 1000 nm. Therefore, the device exhibits applied voltage modulating alternative UV and visible photoresponse. The 350 nm responsivity at −4 V are approximately the same as the peak value at zero bias, which was ascribed to the high probability of electron−hole recombination between the narrow "interface" bandgap, though the reverse applied voltage can expel the generated holes. It should be noted that the peak appears around 500 nm and shows a weak response in the long wavelength portion of the spectrum, indicating a very low

DOI: 10.1021/acsami.5b04287
ACS Appl. Mater. Interfaces 2015, 7, 16653−16658

collection efficiency in this range,[32] which can be attributed to the light with longer wavelength was mainly absorbed in the bulk CZTS; the light-generated carriers were easily recombined in the bulk during the transport process.[33] Time-dependent response of the device was measured under zero bias with turning on and off as 370 nm light irradiated on the device. As shown in the inset of Figure 4b, upon illumination, the photocurrent increased to a value of 1.8 μA. As turn the light off, it decreased to initial value dramatically, indicating that the device has good reproducible characteristics.

The alternative UV and visible photoresponse mechanism of the p-CZTS/n-GaN heterojunction detector can be understood in terms of the energy band diagram based on Anderson's model and the carrier diffusion process, as shown in Figure 5.

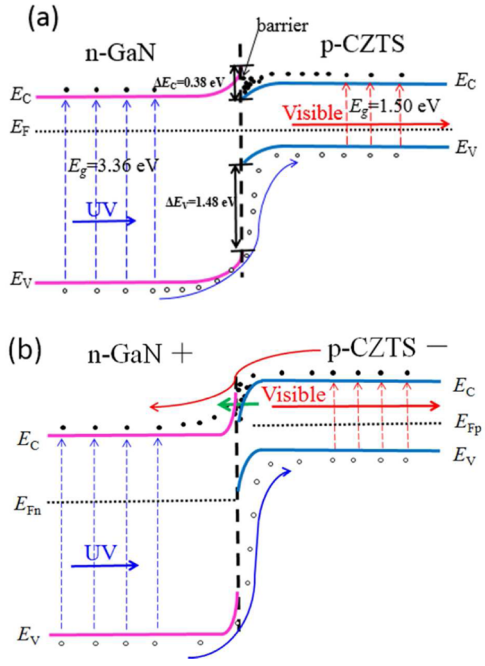

Figure 5. Energy band diagram of the p-CZTS/n-GaN heterojunction with (a) zero and (b) reverse bias, respectively.

The bandgap values of 1.5 and 3.36 eV for the CZTS and GaN are adopted here, respectively, which are calculated from the optical absorption spectra. The electron affinity values are 4.58 eV for CZTS[34] and 4.20 eV for GaN.[35] As the p-type CZTS and n-type GaN are contacted, the model shows a small conduction-band offset of 0.38 eV and a large valence-band offset of 1.48 eV. The energy band diagram of the heterojunction at zero bias is shown in Figure 5a. When the heterojunction is irradiated by the UV light, the photons with energy larger than the bandgap of GaN will be absorbed by the GaN layer. Then electron−hole pairs are photoinduced. The built-in electric field drives the photogenerated holes near or in the junction region toward the CZTS side. In other words, the UV photogenerated holes and electrons were separated, so photocurrent signals can be obtained. When the heterojunction is irradiated by visible light, photons will pass through the GaN layer and be absorbed by the CZTS layer to generate carriers. However, the electrons are confined in the CZTS layer and cannot transfer to the GaN side due to the crack barrier at the interface induced by the positive conduction-band offset. The generated holes cannot drift toward the GaN side to form current for the effect of the electric field and its low mobility and short lifetime. As a result, no photocurrent signals can be detected in this case.

Figure 5b shows the energy diagram of the heterojunction applied with a reverse bias. The visible light arriving at the junction will pass through the GaN layer and be absorbed in the p-CZTS to generate electron−hole pairs. It is noted that the conduction band of the CZTS is higher than that of the GaN. Hence, the visible light-generated electrons in the CZTS layer can tunnel toward the GaN side, and the holes are confined in the CZTS layer due to the larger barrier height. Therefore, there is a wide photoresponse signal range in the visible band. When UV light shines on the junction, the GaN layer will absorb the light and generate electrons and holes. The electric field caused by reverse bias in the depletion region is consistent with the built-in electric field. The photogenerated holes drift easier toward the CZTS layer compared with the zero bias by the strong electric field. However, the smaller "interface" bandgap at the interface, which is defined as the difference between conduction-band minimum (CBM) of the GaN layer and valence-band maximum (VBM) of the CZTS layer, results in the increase of probability of electron−hole recombination. In the CZTS-based solar cells, it is known that the CBM of the CdS buffer located below that of the CZTS and this is equivalent to an "interface" bandgap reduction which favors the interface recombination processes, especially for the recombination between electrons in the conduction band of the buffer layer and holes in the valence band, and influence the V_{oc} of the CZTS/CdS solar cells.[36,37] In our case, the reverse biases applied also induce an "interface" bandgap reduction which will enhance the electron−hole recombination between the "interface" bandgap, so the decrease of efficiency of photon-generated carrier separation causes a weak UV response under reverse biases.

CONCLUSIONS

In summary, we fabricated a p-CZTS/n-GaN heterojunction photodetector and investigated its performance. The heterojunction photodetector shows obvious rectifying behavior. An alternative UV and visible photoresponse was observed via modulating applied bias. Although the intensity of photoresponse is low, our results suggest the p-CZTS/n-GaN heterojunction can be effectively applied in the field of UV/visible photodetector if the quality of the device is further improved.

AUTHOR INFORMATION

Corresponding Authors

*E-mail: liyongfeng@jlu.edu.cn.
*E-mail: binyao@jlu.edu.cn.

Notes

The authors declare no competing financial interest.

ACKNOWLEDGMENTS

This work is supported by the National Natural Science Foundation of China under Grants 10874178, 11074093, 61205038, and 11274135, Specialized Research Fund for the Doctoral Program of Higher Education under Grant 20130061130011, Ph.D. Programs Foundation of Ministry of Education of China under Grant 20120061120011, Natural Science Foundation of Jilin Province under Grant 201115013, and National Fund for Fostering Talents of Basic Science under Grant J1103202.

DOI: 10.1021/acsami.5b04287
ACS Appl. Mater. Interfaces 2015, 7, 16653−16658

REFERENCES

(1) Sheikh, A. D.; Bera, A.; Haque, M. A.; Rakhi, R. B.; Gobbo, S. D.; Alshareef, H. N.; Wu, T. Atmospheric Effects on the Photovoltaic Performance of Hybrid Perovskite Solar Cells. *Sol. Energy Mater. Sol. Cells* **2015**, *137*, 6−14.

(2) Panwar, N. L.; Kaushik, S. C.; Kothari, S. Role of Renewable Energy Sources in Environmental Protection: A review. *Renewable Sustainable Energy Rev.* **2011**, *15*, 1513−1524.

(3) Absi Halabi, M.; Al-Qattan, A.; Al-Otaibi, A. Application of Solar Energy in the Oil Industry Current Status and Future Prospects. *Renewable Sustainable Energy Rev.* **2015**, *43*, 296−314.

(4) Wang, G.; Zhao, W.; Cui, Y.; Tian, Q.; Gao, S.; Huang, L.; Pan, D. Fabrication of a $Cu_2ZnSn(S,Se)_4$ Photovoltaic Device by a Low-toxicity Ethanol Solution Process. *ACS Appl. Mater. Interfaces* **2013**, *5*, 10042−10047.

(5) Liu, Z.; Li, Y.; Liu, C.; Ya, J.; E, L.; Zhao, W.; Zhao, D.; An, L. TiO(2) Photoanode Structure with Gradations in V Concentration for Dye-sensitized Solar Cells. *ACS Appl. Mater. Interfaces* **2011**, *3*, 1721−1725.

(6) Guo, S.; Cao, B.; Wang, W.; Moulin, J. F.; Muller-Buschbaum, P. Effect of Alcohol Treatment on the Performance of PTB7:PC71BM Bulk Heterojunction Solar Cells. *ACS Appl. Mater. Interfaces* **2015**, *7*, 4641−4649.

(7) Jin, K. X.; Li, Y. F.; Wang, Z. L.; Peng, H. Y.; Lin, W. N.; Kyaw, A. K. K.; Jin, Y. L.; Jin, K. J.; Sun, X. W.; Soci, C.; Wu, T. Tunable Photovoltaic Effect and Solar Cell Performance of Self-doped Perovskite $SrTiO_3$. *AIP Adv.* **2012**, *2*, 042131.

(8) Bera, A.; Wu, K.; Sheikh, A.; Alarousu, E.; Mohammed, O. F.; Wu, T. Perovskite Oxide $SrTiO_3$ as an Efficient Electron Transporter for Hybrid Perovskite Solar Cells. *J. Phys. Chem. C* **2014**, *118*, 28494−28501.

(9) Scragg, J. J.; Ericson, T.; Fontané, X.; Izquierdo-Roca, V.; Pérez-Rodríguez, A.; Kubart, T.; Edoff, M.; Platzer-Björkman, C. Rapid Annealing of Reactively Sputtered Precursors for Cu_2ZnSnS_4 Solar Cells. *Prog. Photovoltaics* **2014**, *22*, 10−17.

(10) Xiao, Z.-Y.; Li, Y.-F.; Yao, B.; Deng, R.; Ding, Z.-H.; Wu, T.; Yang, G.; Li, C.-R.; Dong, Z.-Y.; Liu, L.; Zhang, L.-G.; Zhao, H.-F. Bandgap Engineering of $Cu_2Cd_xZn_{1-x}SnS_4$ Alloy for Photovoltaic Applications: A Complementary Experimental and First-principles Study. *J. Appl. Phys.* **2013**, *114*, 183506.

(11) Brammertz, G.; Buffiére, M.; Oueslati, S.; ElAnzeery, H.; Ben Messaoud, K.; Sahayaraj, S.; Köble, C.; Meuris, M.; Poortmans, J. Characterization of Defects in 9.7% Efficient $Cu_2ZnSnSe_4$-CdS-ZnO Solar Cells. *Appl. Phys. Lett.* **2013**, *103*, 163904.

(12) Ge, J.; Chu, J.; Jiang, J.; Yan, Y.; Yang, P. Characteristics of In-Substituted CZTS Thin Film and Bifacial Solar Cell. *ACS Appl. Mater. Interfaces* **2014**, *6*, 21118−21130.

(13) Zeng, X.; Tai, K. F.; Zhang, T.; Ho, C. W. J.; Chen, X.; Huan, A.; Sum, T. C.; Wong, L. H. $Cu_2ZnSn(S,Se)_4$ Kesterite Solar Cell with 5.1% Efficiency Using Spray Pyrolysis of Aqueous Precursor Solution Followed by Selenization. *Sol. Energy Mater. Sol. Cells* **2014**, *124*, 55−60.

(14) Shin, B.; Gunawan, O.; Zhu, Y.; Bojarczuk, N. A.; Chey, S. J.; Guha, S. Thin Film Solar Cell with 8.4% Power Conversion Efficiency Using an Earth-Abundant Cu_2ZnSnS_4 Absorber. *Prog. Photovoltaics* **2013**, *21*, 72−76.

(15) Chen, G.; Yuan, C.; Liu, J.; Huang, Z.; Chen, S.; Liu, W.; Jiang, G.; Zhu, C. Fabrication of Cu_2ZnSnS_4 Thin Films Using Oxides Nanoparticles Ink for Solar Cell. *J. Power Sources* **2015**, *276*, 145−152.

(16) Duan, H.-S.; Yang, W.; Bob, B.; Hsu, C.-J.; Lei, B.; Yang, Y. The Role of Sulfur in Solution-Processed $Cu_2ZnSn(S,Se)_4$ and its Effect on Defect Properties. *Adv. Funct. Mater.* **2013**, *23*, 1466−1471.

(17) Kim, J.; Hiroi, H.; Todorov, T. K.; Gunawan, O.; Kuwahara, M.; Gokmen, T.; Nair, D.; Hopstaken, M.; Shin, B.; Lee, Y. S.; Wang, W.; Sugimoto, H.; Mitzi, D. B. High Efficiency $Cu_2ZnSn(S,Se)_4$ Solar Cells by Applying a Double In_2S_3/CdS Emitter. *Adv. Mater.* **2014**, *26*, 7427−7431.

(18) Tao, J.; Liu, J.; He, J.; Zhang, K.; Jiang, J.; Sun, L.; Yang, P.; Chu, J. Synthesis and Characterization of Cu_2ZnSnS_4 Thin Films by the Sulfurization of Co-Electrodeposited Cu−Zn−Sn−S Precursor Layers for Solar Cell Applications. *RSC Adv.* **2014**, *4*, 23977.

(19) Larramona, G.; Bourdais, S.; Jacob, A.; Choné, C.; Muto, T.; Cuccaro, Y.; Delatouche, B.; Moisan, C.; Péré, D.; Dennler, G. Efficient Cu_2ZnSnS_4 Solar Cells Spray Coated from a Hydro-Alcoholic Colloid Synthesized by Instantaneous Reaction. *RSC Adv.* **2014**, *4*, 14655.

(20) Aizawa, T.; Tanaka, K.; Tagami, K.; Uchiki, H. Investigation of ZnO:Al Window Layer of Cu_2ZnSnS_4 Thin Film Solar Cells Prepared By Non-Vacuum Processing. *Phys. Status Solidi C* **2013**, *10*, 1050−1054.

(21) Gurav, K. V.; Shin, S. W.; Patil, U. M.; Deshmukh, P. R.; Suryawanshi, M. P.; Agawane, G. L.; Pawar, S. M.; Patil, P. S.; Lee, J. Y.; Lokhande, C. D.; Kim, J. H. Cu_2ZnSnS_4 (CZTS)-Based Room Temperature Liquefied Petroleum Gas (LPG) Sensor. *Sens. Actuators, B* **2014**, *190*, 408−413.

(22) Yang, G.; Li, Y.-F.; Yao, B.; Ding, Z.-H.; Deng, R.; Qin, J.-M.; Fang, F.; Fang, X.; Wei, Z.-P.; Liu, L. Band Alignments at Interface of Cu_2ZnSnS_4/ZnO Heterojunction: An X-ray Photoelectron Spectroscopy and First-Principles Study. *J. Alloys Compd.* **2015**, *628*, 293−297.

(23) Htay, M. T.; Hashimoto, Y.; Momose, N.; Sasaki, K.; Ishiguchi, H.; Igarashi, S.; Sakurai, K.; Ito, K. A Cadmium-Free Cu_2ZnSnS_4/ZnO Hetrojunction Solar Cell Prepared by Practicable Processes. *Jpn. J. Appl. Phys.* **2011**, *50*, 032301.

(24) Chen, C.-H.; Chang, S.-J.; Chang, S.-P.; Li, M.-J.; Chen, I. C.; Hsueh, T.-J.; Hsu, C.-L. Novel Fabrication of UV Photodetector Based on ZnO Nanowire/p-GaN Heterojunction. *Chem. Phys. Lett.* **2009**, *476*, 69−72.

(25) Xu, G. Y.; Salvador, A.; Kim, W.; Fan, Z.; Lu, C.; Tang, H.; Morkoç, H.; Smith, G.; Estes, M.; Goldenberg, B.; Yang, W.; Krishnankutty, S. High speed, Low noise Ultraviolet Photodetectors Based on GaN p-i-n and AlGaN(p)-GaN(i)-GaN(n) Structures. *Appl. Phys. Lett.* **1997**, *71*, 2154.

(26) Lin, F.; Chen, S.-W.; Meng, J.; Tse, G.; Fu, X.-W.; Xu, F.-J.; Shen, B.; Liao, Z.-M.; Yu, D.-P. Graphene/GaN Diodes For Ultraviolet and Visible Photodetectors. *Appl. Phys. Lett.* **2014**, *105*, 073103.

(27) Su, L.; Zhang, Q.; Wu, T.; Chen, M.; Su, Y.; Zhu, Y.; Xiang, R.; Gui, X.; Tang, Z. High-Performance Zero-Bias Ultraviolet Photodetector Based on p-GaN/n-ZnO Heterojunction. *Appl. Phys. Lett.* **2014**, *105*, 072106.

(28) Szyszka, A.; Lupina, L.; Lupina, G.; Schubert, M. A.; Zaumseil, P.; Haeberlen, M.; Storck, P.; Thapa, S. B.; Schroeder, T. Ultraviolet GaN Photodetectors on Si Via Oxide Buffer Heterostructures with Integrated Short Period Oxide-Based Distributed Bragg Reflectors and Leakage Suppressing Metal-Oxide-Semiconductor Contacts. *J. Appl. Phys.* **2014**, *116*, 083108.

(29) Ahmed, S.; Reuter, K. B.; Gunawan, O.; Guo, L.; Romankiw, L. T.; Deligianni, H. A High Efficiency Electrodeposited Cu_2ZnSnS_4 Solar Cell. *Adv. Energy Mater.* **2012**, *2*, 253−259.

(30) Anh Tuan, T. T.; Kuo, D.-H. Temperature-Dependent Electrical Properties of the Sputtering-Made n-InGaN/p-GaN Junction Diode with a Breakdown Voltage above 20V. *Mater. Sci. Semicond. Process.* **2015**, *32*, 160−165.

(31) Ding, M.; Zhao, D.; Yao, B.; Li, Z.; Xu, X. Ultraviolet Photodetector Based on Heterojunction of n-ZnO Microwire/p-GaN Film. *RSC Adv.* **2015**, *5*, 908−912.

(32) Jheng, B.-T.; Chen, I. P.; Wu, M.-C. Electrical and Optical Properties of Cu_2ZnSnS_4 Films with Different Chemical Composition. *Sci. Adv. Mater.* **2015**, *7*, 233−238.

(33) Kim, K.; Kim, I.; Oh, Y.; Lee, D.; Woo, K.; Jeong, S.; Moon, J. Influence of Precursor Type on Non-Toxic Hybrid Inks for High-Efficiency Cu_2ZnSnS_4 Thin-Film Solar Cells. *Green Chem.* **2014**, *16*, 4323.

(34) Avellaneda, D.; Nair, M. T. S.; Nair, P. K. Cu_2SnS_3 and Cu_4SnS_4 Thin Films via Chemical Deposition for Photovoltaic Application. *J. Electrochem. Soc.* **2010**, *157*, D346.

(35) Soylu, M.; Yakuphanoglu, F. Properties of Sol−Gel Synthesized n-ZnO/n-GaN (0001) Isotype Heterojunction. *Mater. Chem. Phys.* **2014**, *143*, 495−502.

DOI: 10.1021/acsami.5b04287
ACS Appl. Mater. Interfaces 2015, 7, 16653−16658

(36) Santoni, A.; Biccari, F.; Malerba, C.; Valentini, M.; Chierchia, R.; Mittiga, A. Valence Band Offset at the CdS/ Cu_2ZnSnS_4 Interface Probed by X-ray Photoelectron Spectroscopy. *J. Phys. D: Appl. Phys.* **2013**, *46*, 175101.
(37) Yin, L.; Cheng, G.; Feng, Y.; Li, Z.; Yang, C.; Xiao, X. Limitation Factors for the Performance of Kesterite Cu_2ZnSnS_4 Thin Film Solar Cells Studied by Defect Characterization. *RSC Adv.* **2015**, *5*, 40369−40374.

DOI: 10.1021/acsami.5b04287
ACS Appl. Mater. Interfaces 2015, 7, 16653−16658